Modeling the Effects of Torsional Disorder on the Spectra of Poly- and Oligo-(*p*-phenyleneethynylenes)†

Lu Tian Liu and David Yaron*

Department of Chemistry, Carnegie Mellon University, Pittsburgh, Pennsylvania 15213

Mikhail I. Sluch and Mark A. Berg

Department of Chemistry and Biochemistry, University of South Carolina, Columbia, South Carolina 29208

Received: October 31, 2005; In Final Form: February 22, 2006

The absorption spectra of phenyleneethynylene oligomers show an unusual change in shape with oligomer length. The unusual aspects of the spectra arise from rotation of the phenylene rings about the long axis of the oligomer. In the ground electronic state, the barrier to this rotation is low and the spectra in room temperature come from an ensemble of different structures. In the excited electronic state, the barrier to rotation is substantially higher, giving rise to strong nonlinear electron−phonon coupling. A multidimensional semiempirical model that includes these effects is developed for the photophysics of phenyleneethynylene oligomers. The ground-state energy is modeled with a molecular mechanics expression, and the excitation energy is modeled with an exciton model. Intermediate Neglect of Differential Overlap/Singles Configuration Interaction (INDO/SCI) calculations verify the exciton model and provide initial estimates of the model parameters. These parameters generate the qualitative features seen in experimental spectra. Inclusion of entropy effects from the multiple torsional coordinates is essential. Refinement of the parameters yields quantitative agreement with experiment. This agreement shows that coupling to torsional motion is a major factor in the spectroscopy and photophysics of these conjugated polymers.

I. Introduction

p-Phenyleneethynylene oligomers and polymers (PPEs), shown in Figure 1, are commonly used as "molecular wires" due to their high degree of conjugation and rigid, linear structure.[1−4]

Their optical spectra show a strong asymmetry between absorption and emission, which is unusual for most compounds. On the basis of spectral measurements vs temperature, viscosity, and time-resolved fluorescence on a single oligomer, two of us proposed that this asymmetry is due to strong quadratic coupling between the electronic transition and torsional motion of the rings around the backbone.[5]

Although the spectral anomalies in PPE are particularly dramatic and well documented, the essential feature of strong asymmetry in the shapes of absorption and emission have been observed in a variety of conjugated polymers: PP (oligophenylenes),[6,7] PPV (polyphenylenevinylene) polymers[8] and oligomers,[9,10] oligofluorenes,[11−13] and oligothiophenes.[14] The oligomer results are particularly important because they obviate a role for energy migration in causing the spectral asymmetry.[15] The spectral asymmetry in these other systems has also been attributed to nonlinear coupling to nuclear motions.[7,10,16] The models differ as to whether the important nuclear motions are high-frequency vibrational modes or torsions and whether the coupling is quadratic or more highly nonlinear. However, none of these models are capable of a full treatment of all the torsions in a large oligomer.

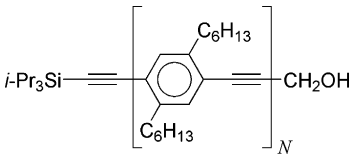

Figure 1. Structure of the (*p*-)phenyleneethynylene oligomers (PPEs).

This paper identifies a new spectral anomaly in PPE: the absorption spectra show striking changes in shape as a function of oligomer length. This feature is not explained by the quadratic-coupling model suggested earlier.[5] Here, an exciton model for the effect of torsions on the electronic state is developed that is able to quantitatively explain the observed spectra. In addition to providing a full treatment of the nonlinearity of the torsional potential, this model includes the full multidimensionality of the torsional motion in longer oligomers. This multidimensionality is an essential feature of the model.

The standard model for the coupling of nuclear motion and electronic states assumes linear electron−phonon coupling and harmonic nuclear motion, as illustrated in parts a and b of Figure 2.[17] The essential features of this model are unchanged whether the nuclear motion is treated classically or quantum mechanically or whether the nuclear motion is an intramolecular motion, a phonon of the matrix, or a solvent reorganization. The nuclear motion in each electronic state is assumed to be harmonic with the same force constant. The displacement of the minima of the two potential curves represents a linear coupling, that is, the difference between the two potentials is linear in the nuclear coordinate. Mixing of different nuclear coordinates (Duschinsky rotation[18]) is ignored.

† Part of the special issue "Robert J. Silbey Festschrift".

* To whom correspondence should be addressed. E-mail: yaron@chem.cmu.edu.

10.1021/jp056284x CCC: $33.50
Published on Web 04/22/2006

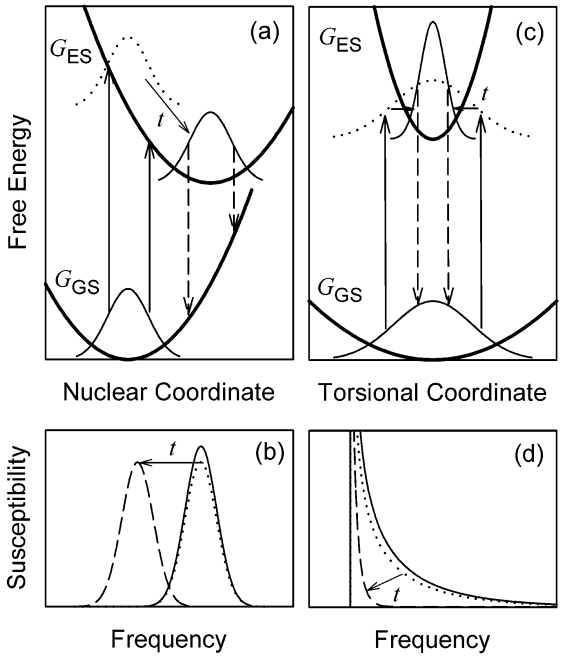

Figure 2. Schematic illustrations of the linear (a and b) and quadratic (c and d) models for coupling of an electronic transition to a single nuclear coordinate. The effective ground (G_{GS}) and excited (G_{ES}) state potentials are shown as heavy curves in (a) and (c). The ground-state population distributions (curves on G_{GS} in (a) and (c)), absorption width (arrows in a and c), and absorption spectra (curves in b and d) are shown as solid lines. The corresponding features of the relaxed ES are shown as dashed lines; those of the unrelaxed ES are shown as dotted lines. With linear coupling, the absorption and emission spectra are shifted but have the same broadening. In quadratic coupling, there is no shift between the peaks of the absorption and emission spectra, but the relaxed emission spectrum is narrower than the absorption spectrum.

For a low-frequency, classical nuclear motion, such as a ring torsion, this linear-coupling model predicts Gaussian line shapes of identical width in both absorption and emission. There is a shift between the peaks of the line shapes, the Stokes shift, that is directly proportional to the square of the Gaussian's full width at half maximum (fwhm). In time-resolved emission, the Gaussian emission line shifts toward lower frequency with time but does not change shape. In real systems, this Gaussian broadening from low-frequency motions is superimposed on the vibronic structure of the high-frequency intramolecular vibrations. The linear-coupling model has been very successful in explaining the basic spectroscopy of most organic molecules in the condensed phase.

Sluch et al. observed that the $N = 9$ PPE oligomer in room-temperature solution has a narrow emission spectrum, but a much broader absorption spectrum, in clear disagreement with the linear-coupling model.[5] They also found that the time-resolved emission showed no shift of the peak frequency, but rather an asymmetric narrowing of an exponential tail on the emission line, another clear violation of the linear-coupling model. They also noted that the emission spectrum broadens in viscous solutions and that the absorption and emission spectrum becomes approximately mirror symmetric in a rigid glass. The strong influence of solvent viscosity implicates large amplitude torsions, rather than high-frequency vibrations, as the origin of this effect.

For PPEs in their ground electronic state, the bonds connecting the phenylene groups have primarily single-bond character and the barrier to rotation of the phenylene rings about the long axis of the oligomer is near *kT*. The first excited state (ES) contains more quinoidal/cumulenic character, and the rotational barrier is significantly higher than that in the ground state (GS).

Sluch et al. proposed that this effect leads to large quadratic coupling between the electronic excitation and torsional motions, as illustrated in parts c and d of Figure 2. In a quadratic-coupling model, the ground and excited states are harmonic and have minima at the same position but have different curvatures and thus different vibrational frequencies in the ground and excited states.[19,20] In the current case, both the GS and ES have their minima at zero torsional angle but the ES is more tightly constrained to planarity than the GS. As a result, there is a wide range of torsional angles in the GS, and the absorption spectrum is broad. Immediately following excitation, the excited state has the same wide range of torsional angles. If torsional rotation is allowed, then the excited-state population relaxes to a much narrower range of angles and the emission spectrum is narrow. However, in rigid media, torsional relaxation cannot occur, so the emission spectrum remains as broad as the absorption spectrum. Thus, this simple model qualitatively explains the observed features of the steady-state spectra. Sluch et al. also observed the asymmetric narrowing of the emission spectrum with time that is predicted by this model.

In this paper, we examine the absorption spectra of a series of oligomers, $N = 2$, 3, 4, 9, and the polymer. The absorption spectra show an unusual evolution of shape with increasing chain length (section II). The spectrum is sharp for $N = 2$, shows apparent additional peaks or shoulders for $N = 3$ and 4, and then partially narrows again for $N = 9$ and the polymer. This behavior cannot be explained by the simple model of parts c and d of Figure 2 , nor is it explained by other treatments of electron−phonon coupling in conjugated polymers.[7,10,16]

To explain these results, we develop a multidimensional torsional model with potentials derived from electronic structure calculations (section III). This model assumes that an exciton hops coherently between adjacent repeat units, with a transfer amplitude that depends on the torsional angle between rings. The model is parametrized to results from Intermediate Neglect of Differential Overlap/Singles Configuration Interaction (INDO/SCI) calculations on about 2000 representative structures. This exciton model is efficient enough to allow a large ensemble of torsional configurations to be sampled, even in the long oligomer. Without adjusting the model, the important features of the experimental spectra are reproduced.

More quantitative comparison of the model and experiment requires refinement of the model parameters and a detailed consideration of the vibronic structure (section IV). With modest and reasonable adjustments, the observed spectra are reproduced in detail. As a result, it is clear that torsional motion is the dominant factor in the spectral shapes of PPEs and an exciton model can accurately describe the interaction of this motion with the electronic states. This approach should also be useful for the more general description of the photophysics of these and other conjugated polymers.

II. Experimental Results

The synthesis of the oligomers of 2,5-dihexyl-*p*-phenyleneethynylene in Figure 1 with $N = 2$, 3, 4, and 9 has been described by Ziener and Godt.[21] The corresponding methyl-terminated polymer with an estimated average $N = 100$ was prepared by the method of Bunz and co-workers.[22,23] Solutions were prepared in chloroform. Aggregates, which are identifiable by their red-shifted absorption,[24] were permanently eliminated by heating the solutions briefly to their boiling points.

Emission spectra were taken of solutions dilute enough to prevent reabsorption of the red edge of the emission and to

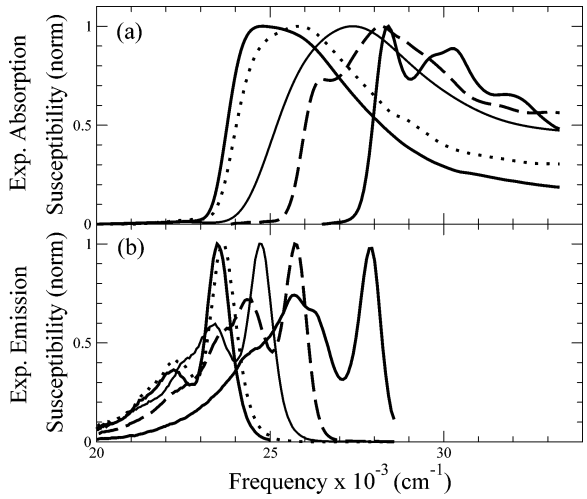

Figure 3. Experimental absorption (a) and emission (b) spectra of the PPE oligomers of Figure 1, in room-temperature chloroform. Right to left in both panels: $N = 2$ (solid), $N = 3$ (dash), $N = 4$ (thin solid), $N = 9$ (dot), and polymer ($N \sim 100$, solid).

prevent reformation of aggregates. Spectra were taken with 1 nm excitation and emission bandwidths and with magic angle polarizations. In these low viscosity solutions, the emission spectrum is independent of the excitation frequency. The frequency-dependent sensitivity of the fluorescence spectrometer was calibrated using a standard lamp, and the results were used to correct the emission intensity, I_λ, to radiometric units (proportional to W/nm).[25]

The emission and corresponding absorption spectra of several oligomers ($N = 2$, 3, 4, and 9) and the polymer are compared in Figure 3. These spectra are consistent with previous reports on PPE oligomer spectra.[26,27] The spectra are presented as susceptibility χ vs frequency ν ($\chi \propto \epsilon_{abs}$ or $\chi \propto I_p(\nu)/\nu^3$ and $I_p(\nu) \propto I_\lambda(\lambda)/\nu^3$).[28] These units facilitate quantitative comparison of absorption, emission, and calculated spectra. Susceptibilities are directly proportional to the initial-state population, final-state density of states, transition dipole moment, and Franck−Condon factor, without any explicit frequency factors. If the transition moment is independent of the nuclear coordinates, and if the vibronic transitions are treated as harmonic oscillators displaced by the electronic transition, then the absorption and emission susceptibility spectra will be mirror images. This result does not hold quantitatively for spectra displayed using absorbance, fluorescence intensity, or wavelength scales.

The emission spectra in Figure 3b are readily understood. The prominent and narrow $0 \rightarrow 0$ band shows a shift toward lower frequency with increasing polymer length. The shift is linear in $1/N$, until approximately $N = 10$, beyond which the polymer shows no further shift. This effective conjugation length is longer than the longest oligomer examined. Thus, energy migration between different conjugated segments on the same oligomer will not occur for the oligomers considered here.

In addition to the $0 \rightarrow 0$ band, each of the emission spectra show vibronic bands at lower frequency. The relative intensity of the higher vibronic bands decreases with oligomer length, as expected.[29]

Unlike the emission spectra, the absorption spectra (Figure 3a) are difficult to interpret from standard theory. For $N = 2$, the vibronic transitions seen in the emission spectrum are also identifiable in the absorption spectrum, but the two spectra are not truly mirror symmetric. For the longer oligomers, the vibronic structure is lost; the absorption spectra show an additional broadening that is not present in the emission spectra. The polymer and $N = 9$ oligomer absorption spectrum could be described roughly as the convolution of a Gaussian with the corresponding emission spectrum. However, the $N = 4$ and $N = 3$ spectra are even broader than the spectra of the longer oligomers. The $N = 3$ spectrum even shows a low-frequency peak. If this peak were a vibronic peak, then it is hard to understand why it survives despite the strong broadening of the rest of the spectrum.

Standard models based on linear coupling of the electronic transition cannot explain these results. They predict equal and symmetric broadening of the absorption and emission spectra. Moreover, they predict that any source of broadening will also cause a shift of the emission spectrum to lower frequency as in Figure 2b. Despite the broadening of the absorption spectra in Figure 3, the peak emission frequency is shifted by very little from the onset of absorption.

The quadratic-coupling model can roughly explain the $N = 2$ spectra. This model predicts a broad absorption spectrum, a narrow emission spectrum, and peaks of the two spectra at the same frequency. The experimental spectra for $N = 2$ do indeed have a resolved absorption spectrum, a broadened absorption spectrum, and a very small Stokes shift. In the quadratic-coupling model, the absorption spectrum is strongly broadened toward high frequencies, but has a sharp cusp at low frequencies, as shown in Figure 2d. When this type of broadening is convolved with the underlying vibronic structure of the spectrum, the cusp from each transition leads to a resolved structure, but the broad tails of the broadening function lead to a high level of unstructured intensity at higher frequencies. Consistent with this model, the experimental $N = 2$ absorption spectrum shows sharp vibronic peaks on top of a broad unresolved background.

Although the previously proposed quadratic-coupling model explains the $N = 2$ spectra, at least at a qualitative level, it does not explain the changes in the broadening seen for longer oligomers. For this reason, we developed a model of oligomer spectra that explicitly includes the multidimensionality of the torsional modes for longer oligomers and that bases the form of the torsional potentials on explicit electronic structure calculations.

III. Simulation of Spectra

A. Averaging over Torsional Configurations. Absorption spectra are simulated by generating a set of torsional configurations. Each configuration, A, is described by a set of dihedral angles, $\{\theta_j\}$, where j specifies the torsional angle between the jth and $(j + 1)$th phenylene rings. The ensemble is defined by the Boltzmann probability

$$P_A \propto \exp\left(-\frac{E_{GS}(A)}{kT}\right) \tag{1}$$

where A indexes a particular configuration, $E_{GS}(A)$ is the energy of the ground electronic state for a given configuration, k is the Boltzmann constant, and T is the temperature taken as 298 K throughout this study.

We assume the oligomer remains linear, with bond lengths and nontorsional bond angles independent of both torsional angles and oligomer length. Figure 4 shows the bond lengths and bond angles used in the model. These values are taken from a geometry optimization performed using density functional theory in the GAUSSIAN program, (B3LYP/3-21G).[30] The results are similar to the literature-reported data.[31]

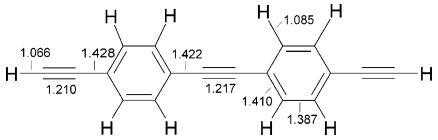

Figure 4. PPE oligomer geometry used in the INDO/SCI calculations.

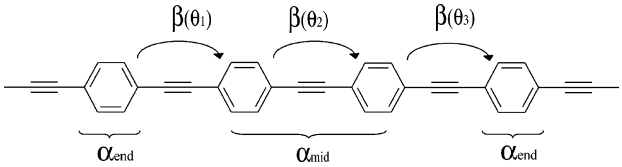

Figure 5. Schematic representation of the exciton model used to calculate the excitation energy. α is the energy of the exciton on a particular site, β is the transfer amplitude between neighboring sites, and θ is the dihedral angle.

Spectra are obtained by randomly generating 100 000 configurations, using a uniform random number generator for θ_j, and summing the spectra associated with these configurations assuming the Boltzmann weighting factor of eq 1

$$I(\omega) = \sum_A P_A I(\omega, A) \tag{2}$$

where $I(\omega, A)$ is the spectrum for configuration A.

B. Ground-state Energy. The energy of the ground electronic state is modeled using a simple molecular mechanics expression[32]

$$E_{GS}(A) = \frac{V}{2} \sum_{j=1}^{N-1} [1 - \cos(2\theta_j)] \tag{3}$$

where V is the rotational barrier, defined as the energy difference between the perpendicular ($\theta = 90°$) and planar ($\theta = 0°$) conformations, and the sum is over the $N - 1$ dihedral angles in an oligomer of length N.

The rotational barrier for tolane (diphenylethynylene) has been measured to be $V_{tolane} = 0.59$ kcal/mol in the gas phase.[32] Tolane consists of two phenyl rings separated by an ethynyl group. It is analogous to the $N = 2$ oligomer studied here, although without the end groups and side chains. In fitting the spectra below, we quote the ground-state barrier in units of the tolane barrier, such that $V = CV_{tolane}$.

The ground-state energy of eq 3 assumes that the various torsions are uncoupled.[33] This assumption is supported by quantum chemical Hartree−Fock calculations performed with the AM1 semiempirical model.[34] For example, for an $N = 4$ oligomer, the ground-state energy difference between $\{\theta_1, \theta_2, 0°\}$ and $\{\theta_1, \theta_2, 90°\}$ varies by less than 1%, as θ_1 and θ_2 are varied from 0° to 90°.

C. Exciton Model for the Excitation Energy. The excitation energy is obtained from a model in which the excitation is treated as a single quantum-mechanical particle, whose wave function and Hamiltonian are expressed in a basis set of excitations localized on individual phenyleneethynylene units. This particle, or exciton, hops coherently between the neighboring sites on an oligomer. In Figure 5, the sites are shown as each of the phenylene rings. We note however that, since the exciton is larger than a single ring, these sites are not literal and the model is meant only to empirically capture the couplings between the various repeat units of the oligomer. Below, we verify this exciton approach by comparison to explicit INDO calculations.

TABLE 1: Parameters Defining the INDO/SCI Data Used to Parameterize the Exciton Model[a]

N	dihedral angles	no. structures
2	0°, 1°, 2°, 3°, ..., 90°	91
3	0°, 5°, 10°, 15°, ..., 90°	190
4	0°, 10°, 20°, 30°, ..., 90°	550
5	0°, 15°, 30°, 45°, ..., 90°	1372

[a] The data set includes all unique structures that can be constructed with torsional angles selected from those listed.

The "on-site" energy, α, is the energy of the excitation on a particular site. α is assumed to be the same for all sites, α_{mid}, except for the end sites, where it has the value α_{end}. The difference between these values, $\alpha_{end} - \alpha_{mid}$, models an increase in the energy of the excitation as it approaches the chain end. The amplitude for coherent hopping between adjacent sites is assumed to depend only on the torsional angle between those sites, $\beta(\theta)$. The Hamiltonian matrix for the excited electronic state is then

$$H = \begin{pmatrix} \alpha_{end} & \beta(\theta_1) & 0 & \cdots & 0 \\ \beta(\theta_1) & \alpha_{mid} & \beta(\theta_2) & 0 & \vdots \\ 0 & \beta(\theta_2) & \ddots & \ddots & 0 \\ \vdots & 0 & \ddots & \alpha_{mid} & \beta(\theta_{N-1}) \\ 0 & \cdots & 0 & \beta(\theta_{N-1}) & \alpha_{end} \end{pmatrix} \tag{4}$$

The relevant, optically bright, ES is taken as the lowest eigenvector of eq 4.

The exciton model is parametrized to explicit quantum chemical calculations (INDO/SCI) by least-squares fitting. Table 1 shows the configurations included in the quantum chemical data set for $N = 2$, 3, 4, and 5. The configurations include all unique structures that can be constructed with torsional angles selected from those listed in the table, with the bond lengths of Figure 4. The INDO/SCI calculations include excitations between all filled and empty orbitals, using a direct SCI approach.[35]

To fit the model to the INDO/SCI results, we treat the value of β at each of the angles in Table 1 as an independent variable, $\beta(\theta_j)$. For $N = 4$, this leads to 10 hopping parameters, $\beta(0°)$, $\beta(10°)$, ..., $\beta(90°)$, along with two "on-site" energy parameters, α_{mid} and α_{end}. These 12 parameters are fit to data from 550 INDO/SCI calculations. For $N = 5$, where θ is incremented in 15° steps, 9 parameters are trained to 1372 points. In all cases, the parametrized exciton model reproduces the INDO/SCI energies to within 200 cm^{-1}.

For the INDO/SCI excitation energies used in model parameter fitting, we consider three different choices: (i) the energy of the lowest ES, (ii) the energy of the state that carries the largest one-photon intensity, and (iii) a weighted average of the energy of states within 1000 cm^{-1} of the most intense state, with the weight being proportional to the intensity.

The left panel of Figure 6 plots the INDO/SCI energy of the six lowest INDO/SCI ESs along with the corresponding optical intensity as a function of dihedral angle for $N = 4$, with all torsional angles being increased in unison. A curve crossing occurs at high torsional angles, such that the lowest ES does not carry the optical intensity for highly twisted configurations. Thus, choice (i) is not appropriate. Choices (ii) and (iii) are more appropriate.

To reinforce this point, the right panel of Figure 6 compares $\beta(\theta)/\beta(0°)$ to the $\cos(\theta)$ dependence expected based on orbital overlap for all three cases.[36] Choice (i) leads to substantial deviation from $\cos(\theta)$ for angles above about 70°, where curve

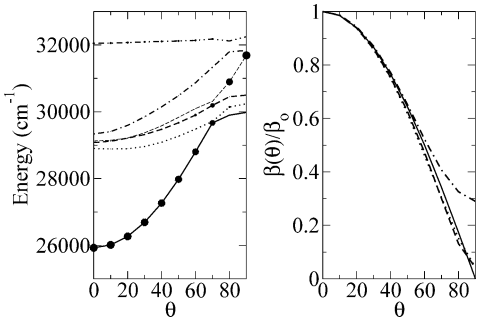

Figure 6. Left panel shows the six lowest ESs from INDO/SCI calculations on a PPE oligomer with $N = 4$, as the dihedral angles θ are increased in unison. The size of the circles are proportional to the optical intensity of the state. The right panel shows the transfer integral, $\beta(\theta)/\beta(0°)$, as a function of θ, obtained using the fitting procedures described in the text. Fits are shown to the state carrying the most intensity (dash), the lowest energy state (dash dot), and the intensity weighted average energy (dot, often overlapping the dashed line). The solid line is $\cos(\theta)$.

TABLE 2: Results from Fitting the Exciton Model of Figure 5 to the INDO/SCI Data of Table 1[a]

chain length	α_{mid}	$\alpha_{end} - \alpha_{mid}$	β_o	rms error
2	32775	0	4391	184
3	32052	−2	3804	89
4	31615	115	3567	93
5	31368	340	3464	80
m	4687	−2454	3143	
b	30448	792	2798	

[a] The model is fit to the INDO/SCI state that carries the highest optical intensity. All quantities are in cm^{-1}, and the rms error refers to the deviation of the exciton model results from the INDO/SCI excitation energy. To obtain the parameters for arbitrary length oligomers, the results are fit to the linear form $P = m^1/_N + b$.

crossings occur in Figure 6. These deviations are much smaller for choices (ii) and (iii).

Choice (iii) was tested in an attempt to improve the prediction of the peak center of the absorption spectrum. However, the results from choices (ii) and (iii) are nearly the same, so the simpler choice (ii) is used for the remainder of this paper.

The results in Figure 6 indicate that it is a good approximation to assume that β of eq 4 is proportional to $\cos(\theta)$

$$\beta = \beta_o \cos(\theta) \tag{5}$$

This allows for a further simplified model with only three parameters, α_{end}, α_{mid}, and β_o. Fitting these three parameters to the data of Table 1 gives the results shown in Table 2.

The model parameters extracted from INDO/SCI on various length oligomers, Table 2, can be fit to a simple linear dependence on $1/N$. This allows the model parameters to be obtained for chain lengths other than those included in the INDO/SCI data set.

D. Predictions of the Torsional Line Broadening. Next, we consider the spectra predicted without introducing any adjustable parameters (Figure 7). We use the ground-state rotational barrier measured for tolane.[32] The parameters for the excitation energy are those of Table 2, obtained from INDO calculations. At this point, only coupling to the torsional motions is modeled. Vibronic transitions due to coupling to higher frequency intramolecular modes are ignored. Thus, the spectra in Figure 7 represent a broadening function to be applied to the vibronic structure from high-frequency modes. The results in Figure 7 can be compared to the low-frequency portion of the

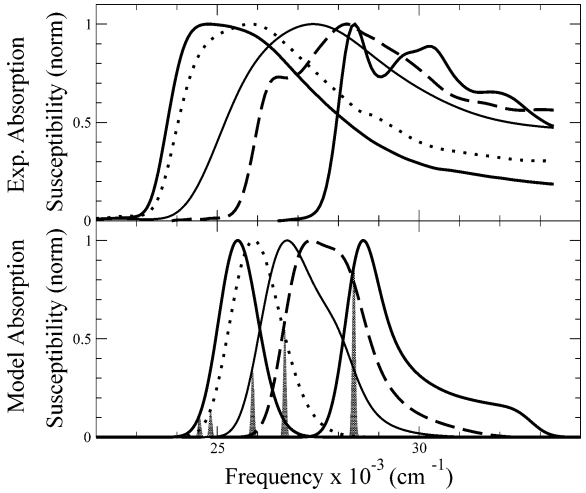

Figure 7. Comparison of experimental (top) and model (bottom) spectra obtained without adjusting model parameters to the experimental spectra and ignoring vibrational structure. A Gaussian homogeneous line width of 500 cm^{-1} is assumed. Right to left in both panels: $N = 2$ (solid), $N = 3$ (dash), $N = 4$ (thin solid), $N = 9$ (dot), and polymer (solid). The narrow Gaussians show the predicted excitation energy of a planar oligomer.

experimental spectra in Figure 3, which are dominated by the broadened $0 \rightarrow 0$ transition.

The predicted spectra show the expected shift to lower frequency with increasing oligomer length, although the red shift is smaller than that seen in experiments. More importantly, the model spectra qualitatively reproduce the unexplained features in the shapes of the experimental spectra. The $N = 2$ spectrum has a low-frequency cusp and a broad high-frequency tail. In the experimental spectra, these features lead to partially resolved vibronic peaks lying on top of a large background of unstructured intensity. In contrast, the $N = 20$ (modeling the polymer) and $N = 9$ spectra show symmetric, Gaussian-like shapes, consistent with the experimental spectra, which are broad and lack any resolved vibronic structure.

The most puzzling feature of the experimental spectra is that the intermediate length oligomers ($N = 3$ and 4) show more broadening than either the shorter or longer oligomers. There is a partially resolved shoulder on the low-frequency edge of the $N = 3$ spectrum. The $N = 4$ spectrum has a very broad low-frequency edge, which could be described as the merging of the shoulder and main peak of the $N = 3$ spectrum.

These features are reproduced by the model. Both the $N = 3$ and $N = 4$ spectra are broader than either the $N = 2$ or $N = 9$ spectra. The broadening has the appearance of an additional poorly resolved peak. Although the relative intensity of the two apparent peaks is not the same as the experimental spectra, we will see in the next section that this problem can be remedied by modest adjustment of the model parameters.

The evolution of the spectra with oligomer length is due to competition between two factors. First, absorption intensity tends to concentrate at low frequencies, because, near the planar configuration, the frequency does not change much for different amounts of torsion. This is the effect that creates a spectral cusp in the quadratic-coupling model. The second factor is the tendency for population to accumulate at higher levels of torsion because of the large number of configurations there, that is, due to an entropy effect.

The entropy effect becomes more important as the number of torsional degrees of freedom increases. The excitation energy of the planar structure is shown as narrow Gaussians in Figure

TABLE 3: Results from Fitting the Emission Spectra of Figure 3 to a Sum of Four Gaussians[a]

chain length	c_1	c_2	c_3	c_4	υ_1	υ_2	υ_3	υ_4	LW_1	LW_2	LW_3	LW_4
2	1.00	0.30	0.24	0.34	0	1611	2207	3115	460	900	1100	2087
3	1.00	0.66	0.35	0.25	0	1271	2191	3198	500	610	500	1000
4	1.00	0.54	0.20	0.13	0	1310	2330	3330	485	730	600	1300
9	1.00	0.38	0.18	0.08	0	1300	2350	3350	500	690	600	500
poly	1.00	0.33	0.18	0.08	0	1240	2220	3220	490	600	600	500

[a] c_i, υ_i, and LW_i are the relative amplitude, offset of the center from the origin in cm^{-1}, and full width of the *i*th Gaussian in cm^{-1}.

7. For $N = 2$, the entropy effect does not exist and the planar peak is prominent. The shape is reminiscent of the highly asymmetric shape predicted by the quadratic-coupling model. For $N = 9$ and 20, the entropy effect is dominant and near planar configurations make little contribution. As expected from the central limit theorem, the shape of the distribution becomes symmetric and Gaussian when a large number of degrees of freedom are involved. In the $N = 3$ and 4 spectra, both the planar peak and the entropy generated peak contribute, leading to broad spectra and apparently structured spectra.

We emphasize that no vibronic transitions are included in the calculations of Figure 7. The appearance of poorly resolved peaks for $N = 3$ and 4 is solely an artifact due to the strong nonlinearity of the electron-torsion coupling and the entropy effect associated with the multidimensionality of the torsional coordinates.

The role of entropy in these spectra and the transition from quadratic-like to linear-like coupling with oligomer length will be discussed in greater detail in a future paper. However, it is clear at this point that, at a qualitative level, the features seen in the experimental spectra are primarily due to coupling to torsional motions.

E. Vibronic Structure. Quantitative comparison of the predicted and measured spectra also requires inclusion of the vibronic structure. For the fits shown next, the vibronic structure is extracted from the experimental emission spectra. In the excited electronic state, the barrier to rotation of the phenylene rings is substantially higher than that in the ground electronic state. The excited state therefore relaxes toward a planar structure, and this causes the emission spectrum to be narrower than the absorption spectrum and to be vibrationally resolved. Table 3 shows the results of fitting the vibronic structure of the emission spectra to a sum of four Gaussians. They roughly correspond to the $0 \rightarrow 0$ transition (υ_1), ring stretching motions (υ_2), acetylenic stretches (υ_3), and a combination of hydrogen stretches and overtones of ring stretches (υ_4).

Figure 8 shows the results of convolving the vibronic structure of each oligomer with the torsional line shape function in Figure 7. For the ground-state rotational barrier, we use the value measured for tolane.[32] The parameters for the excitation energy are those of Table 2, obtained from INDO calculations. There is a discernible similarity between the predicted and observed spectra in Figure 8. However, further optimization of both the model parameters and the vibronic structure is needed.

IV. Empirical Optimization of the Model

The parameters of the exciton model were initially derived from semiempirical calculations on a simplified molecular structure free from solvent. Thus, we expect some error in the quantitative values of these parameters. Quantitative agreement with the experimental spectra will require some empirical adjustment of these parameters. In this section, we look at the assumptions needed to achieve a more detailed agreement with the experiment.

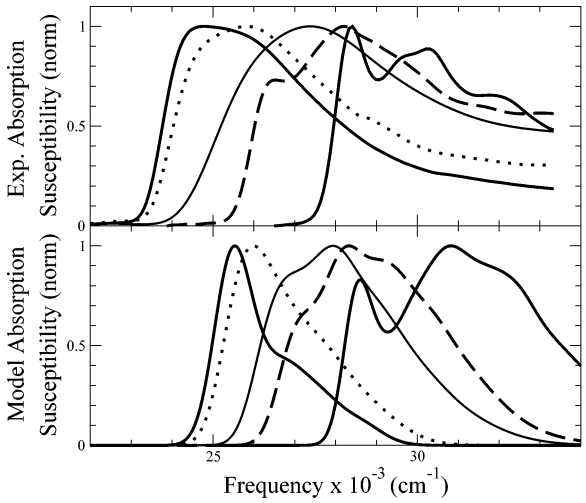

Figure 8. Comparison of experimental (top) and model (bottom) spectra obtained without adjusting model parameters to the experimental spectra and with inclusion of vibronic fine structure. The vibronic structure is extracted from the corresponding experimental emission spectrum. Right to left in both panels: $N = 2$ (solid), $N = 3$ (dash), $N = 4$ (thin solid), $N = 9$ (dot), and polymer (solid).

A. Fitting the $N = 3$ Spectrum. We initially focus on the $N = 3$ oligomer, since the line shape reflects contributions from both the planar cusp and the entropy generated peak. This line shape is therefore quite sensitive to the model parameters. We fit the following three model parameters to the observed spectra: the ground-state rotational barrier, V of eq 3, the excited-state transfer integral, β_o of eq 5, and the homogeneous line width, LW.

The best fit is obtained with a ground-state rotational barrier of 1.18 kcal/mol, which is about twice that of tolane, an ES transfer integral of 1.6 times that from INDO theory, β_o^{INDO} in Table 2, and vibronic line widths equal to those extracted from the emission spectrum of an $N = 3$ oligomer in Table 3. We discuss the sensitivities of the predicted spectrum to each of these parameters in the Supporting Information. The final agreement with the $N = 3$ experimental spectrum is excellent, as shown by the dashed spectra in Figure 9.

B. Fitting the $N \neq 3$ Spectra. We next consider the spectrum as a function of oligomer length. The linear extrapolation of Table 2 can be used to obtain INDO/SCI estimates for the exciton model parameters for any length oligomer. However, in fitting the $N = 3$ spectrum in the previous section, β_o was increased from the INDO/SCI estimate by a scaling factor of 1.6. We consider three means of scaling β_o for chain lengths other than $N = 3$: (a) applying an additive correction, which keeps the slope, *m*, from the INDO/SCI fit and scales only the intercept *b*, (b) applying a multiplicative correction, which scales both the slope and the intercept by a factor of 1.6, or (c) ignoring the dependence on chain length and using the β_o obtained from fitting the $N = 3$ spectrum for all chain lengths.

Finally, a fully quantitative model would need to include the dependence of the vibronic structure on the torsional angles.

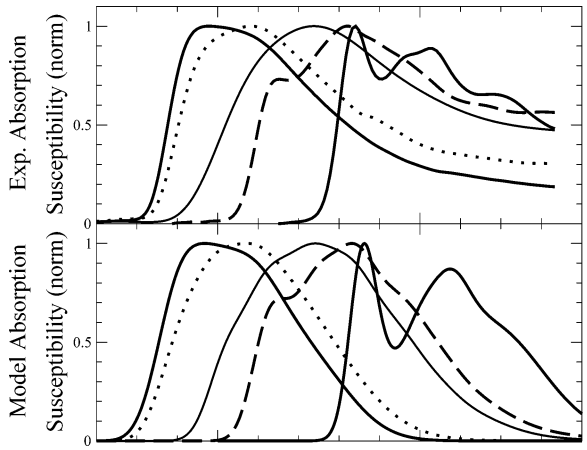

Figure 9. Comparison of experimental (top) and model (bottom) spectra obtained with model parameters fit to the experimental spectra (shown in section IV). Right to left in both panels: $N = 2$ (solid), $N = 3$ (dash), $N = 4$ (thin solid), $N = 9$ (dot), and polymer (solid).

There is experimental evidence (unpublished) that the intensity of the vibronic transitions does in fact change significantly with the degree of torsion in the molecule, with vibronic sidebands becoming more intense as the molecule deviates more strongly from planarity. Thus, the vibronic structure in absorption may differ from the vibronic structure in emission, such that our simulated absorption spectra are expected to underestimate the intensity at higher frequency.

An approximate model for the dependence of the vibronic structure on the torsional angles can be obtained as follows. The disorder present in the thermal ensemble of GS structures tends to localize the exciton, such that the effective conjugation length is less than the physical length of the oligomer. The effects of this localization on the vibronic structure of a long oligomer may be included by using the vibronic structure extracted from the emission spectra of a shorter oligomer. As the exciton becomes more localized, the vibronic coupling increases and the spectrum broadens, which is consistent with the experimental observation that the spectra broaden as the oligomer deviates from planarity.

In fitting the spectra of the $N \neq 3$ oligomers, we adjust three factors. The first factor is which of the above three methods are used to obtain the chain-length dependence of β_o. The best is choice (c). The second factor is the GS barrier for each length oligomer. The best fit is obtained with the barrier set to five times that of tolane for $N = 2$, and twice that of tolane for $N = 3$. For longer chains, it approaches that of tolane (0.59 kcal/mol). The third factor is the oligomer from which the vibronic structure is extracted. The best fits are obtained using the $N = 3$ vibronic structure for all oligomers with $N \geq 3$. (We note however that, since both the GS barrier and the choice of vibronic structure alter the width and vibronic resolution of the predicted spectra, the fit for these two factors are somewhat coupled, making an independent determination problematic.) The Supporting Information examines the sensitivity of the predicted spectra to each of these three factors.

C. Summary of Model Parameters. Figure 9 compares the predictions of the final optimized model with the experimental spectra. The model correctly predicts the overall shift in frequency and change in shape with increasing oligomer length. In the high-frequency tails, the experimental spectra may contain contributions from higher lying states that are not included in the model. However, the shape of the low-frequency edge and peak region of the spectra are modeled very well. Although the model parameters have been empirically adjusted, this agreement supports the basic concepts of the model that the spectral properties of PPEs are dominated by their torsional motions and that an exciton model captures the essential features of the coupling between torsions and electronic excitations. Differences between the experiment and the initial model are due to errors in the quantitative values of the model parameters, not in the basic assumptions of the model.

The fit to the experimental spectrum is quite good, however, the values obtained for the hopping integral β_o and ground-state barrier E_{GS} are somewhat different than expected. INDO/SCI calculations give the hopping integral as $\beta = \beta_o \cos(\theta)$ with $\beta_o = 0.35$ eV. The fit of the experimental $N = 3$ spectrum yields a β_o that is 1.6 times larger than that of INDO/SCI. Although the fit was solely to the $N = 3$ spectrum, the increase in β_o also brings the red shift with increasing chain length into agreement with experiment (compare Figures 7 and 8 with Figure 9). The need to adjust β_o by 60% is somewhat surprising, since INDO theory works quite well for conjugated organic systems.[37−39] INDO/SCI calculations were also used to estimate the dependence of β_o on the length of the oligomer, $d\beta_o/d1/N$. Since β_o must be scaled by 1.6 to obtain agreement with experiment, one might expect a similar scaling to apply to $d\beta_o/d1/N$ (case (b) above). However, a much better agreement with experiment is obtained when $d\beta_o/d1/N$ is unscaled or set to zero (cases (a) and (c) above). Apparently, although INDO/SCI underestimates β_o, it does not underestimate the dependence of β_o on chain length.

Another important model parameter is the rotational barrier in the ground electronic state, E_{GS}, since this establishes the distribution of structures in the thermal ensemble. Microwave experiments find a barrier of 0.59 kcal/mol for tolane in the gas phase.[32] Tolane is a model of the $N = 2$ oligomer studied here, although tolane does not have the end groups or side chains. Semiempirical calculation suggests that this barrier has little dependence on the length of the oligomer and that there is little coupling between the various torsional degrees of freedom present in oligomers with $N > 2$. Our fits to the experimental spectra suggest, however, that the ground-state barrier decreases gradually with oligomer length, from five times that of tolane for $N = 2$ to equal to that of tolane for long oligomers.

V. Discussion

The asymmetry between absorption and emission spectra in PPE is also seen in other conjugated polymers.[8−11,14] One factor that can lead to such asymmetry is energy migration in the excited state,[15] but this is clearly not a factor in the oligomers studied here. Also, since the polymer spectra are a simple extrapolation of the oligomer spectra, energy migration does not appear to be a factor in long PPEs either.

A number of previous studies have treated the asymmetry between absorption and emission spectra in conjugated polymers.[7,10,40] Karabunarliev et al.[40] used a modified quadratic-coupling model that included the change in frequency in the excited state but used linear-coupling results for Franck−Condon factors. Both high-frequency and torsional modes were treated in a number of conjugated polymers, although the authors noted that this method is not quantitative for torsions. Gierschner et al. used a method similar to treat PPV in detail.[10] Heimel et al. treated PP with a fully nonlinear torsional potential and exact quantum Franck−Condon factors.[7] The calculated potential was empirically corrected to obtain agreement with experiment. Both of the latter two studies focused on a single torsional coordinate.

The current study introduces a number of new features. The use of an exciton model parametrized against electronic structure

calculations allows fully nonlinear torsional potentials to be calculated in long oligomers. A semiclassical treatment of the absorption and emission (classical torsional motion with vertical electronic transitions) is substituted for Franck−Condon approaches. This method facilitates the treatment of large systems. It is also more natural in the condensed phase, where torsions do not undergo coherent quantum oscillations. The inclusion of external influences on the torsions, for example, side-chain interactions, or treating dynamics, for example, solvent viscosity, is straightforward in this classical approach. This semiclassical approach has been essential in treating the multidimensional effects that strongly affect the evolution of the absorption line shape with oligomer length.

The strong coupling of the torsions to the electronic transition is due to the change in electronic structure upon excitation to the first ES. The GS is dominated by phenylene/ethynylene configurations. Rotation about the single bonds in these configurations is facile. The ES has a much greater involvement of quinoidal/cumulenic configurations in which the ground-state single bonds pick up double-bond character. As a result, the ES favors planarization of the phenylene rings much more than the GS. In PPE, these effects lead to particularly strong torsional effects on the spectra, because of the very low torsional barrier in the ground state. However, the stiffening of torsions in the excited state is common to many conjugated polymers. In addition, the torsional potentials can be quite flat near planarity, even when the barrier is significant.[40] Thus, the effects seen here may play a role in a wide range of systems.

The exciton model developed here is supported both by explicit INDO/SCI calculations on various length oligomers and by the ability of the model to explain the evolution of the absorption spectra in Figure 9 with chain length. This model has some rather interesting consequences for the excited-state potential energy surface. For instance, consider the barrier to rotation about the central dihedral angle of an oligomer. In the exciton model, rotation of this angle from 0° to 90 ° breaks conjugation, essentially cutting the oligomer in half. The excitation energy of an oligomer of length N thus becomes that of an oligomer of length $N/2$. The excited-state rotational barrier is then the sum of the ground-state barrier and $E_{exc}(N/2) - E_{exc}(N)$, where $E_{exc}(N)$ is the excitation energy of an oligomer with length N. The energy difference $E_{exc}(N/2) - E_{exc}(N)$ decreases with oligomer length, approaching zero for N much greater than the conjugation length of the system. We therefore expect the barrier to rotation about a central dihedral angle to approach the ground-state barrier as the chain length increases. The barrier to rotation therefore depends on the delocalization length of the excitation. More generally, this example illustrates that the barrier to rotation about a particular angle in the excited state may depend on the torsional configuration of the remainder of the oligomer since, for example, this configuration can alter the effective delocalization length of the excited state. The exciton model therefore implies that substantial couplings between nearby torsional angles may be present in the excited state.

A weakness of the current model is the approach used to model the vibronic structure from high-frequency modes. The current model extracts the vibronic structure from the emission spectra. An attempt was made to include coupling between the vibronic structure and the dihedral angles by noting that torsional disorder decreases the effective conjugation length. It may then be appropriate to use the vibronic structure extracted from the emission of an ordered short oligomer to model the vibronic structure of a disordered longer oligomer. The consequences of altering the vibronic structure were examined in detail in the Supporting Information. However, altering the model used for the vibrational fine structure affects the spectrum in a manner that is similar to that resulting from changes in the ground-state barrier. This makes it difficult to independently determine these two parameters. A more sophisticated model for the coupling to high-frequency modes would provide a better estimate of these model parameters.

The effects of other simplifications in the model will likely have a smaller impact than the above. For instance, the side chains on the oligomer are ignored, but since they do not participate in the π-conjugation, they should not have strong effects on the observed spectra. Solvent effects are also ignored, but these are expected to be fairly minor for the low-energy electronic states of a system whose GS and ES have small permanent dipole moments.[41]

Although this paper considers only energy transfer on PPE oligomers, we might expect similar effects to arise in charge transfer through these systems. The origin of the unusual spectra considered here is the large torsional disorder in the ground electronic state and the planarization of the molecule in its excited electronic state. This exciton-induced planarization is due to the ES being more sensitive to conjugation than the GS. Since a free charge on this oligomer would also be more sensitive to conjugation than the uncharged GS, an analogous planarization of the molecule may occur in the presence of a charge. This charge-induced planarization could lead to unusual features in the electron-transfer properties of these molecules.

In a previous paper, two of us suggested the importance of torsional motion in the photophysics of PPEs and proposed a one-dimensional model (1-D) with quadratic coupling to account for the coupling of the torsions to the electronic transition.[5] That model provided a conceptually simple and qualitatively correct explanation for a number of phenomena, including the broadening of the emission spectrum in rigid media, the narrowing of the emission spectrum relative to the absorption spectrum, and the form of the time-resolved emission. However, it does not explain the shape of the absorption spectrum and particularly the change in that shape with oligomer length.

The current model includes a full multidimensional treatment of the torsional motions and replaces the assumption of parabolic energy surfaces with realistic surfaces based on semiempirical calculations. The increase in number of torsional degrees of freedom with oligomer length has strong effects in PPE. In other conjugated oligomers, such as PPP and PPV,[7,11,40,42] torsional motion is also known to contribute to the asymmetry of the line shapes between absorption and emission. Similar effects with increasing chain length may also be expected in such systems, although the magnitudes may be considerably smaller given that the barriers to torsion in the ground state are considerably higher in those systems than in PPE.

In a subsequent paper, we will show that at least semiquantitative accuracy can be achieved by reducing the multidimensional model to a single effective coordinate but retaining the full nonlinearity of the free energy surfaces. This simplified effective 1-D model provides greater insights into the origin of the non-Gaussian line shapes predicted by the full model presented here. We will also consider other systems using this effective 1-D model.

Acknowledgment. We thank Adelheid Godt for providing the oligomer samples and Uwe H. F. Bunz for providing the polymer sample. This work was supported by the National Science Foundation (CHE-0220986 and CHE-0316759).

Supporting Information Available: Figures demonstrating the sensitivity of the predicted spectra to the model parameters. This material is available free of charge via the Internet at http://pubs.acs.org.

References and Notes

(1) Seminario, J. M.; Zacarias, A. G.; Tour, J. M. *J. Am. Chem. Soc.* **1998**, *120*, 3970−3974.

(2) Tour, J. M. *Acc. Chem. Res.* **2000**, *33*, 791−804.

(3) Joachim, C.; Ratner, M. A. *Nanotechnology* **2004**, *15* (8), 1065−1075.

(4) Lee, S.; Thomas, K. R. J.; Thayumanavan, S.; Bardeen, C. J. *J. Phys. Chem. A* **2005**, *109*, 9767−74.

(5) Sluch, M. I.; Godt, A.; Bunz, U. H.; Berg, M. A. *J. Am. Chem. Soc.* **2001**, *123*, 6447−6448.

(6) Momicchioli, F.; Bruni, M. C.; Baraldi, I. *J. Phys. Chem.* **1972**, *76*, 3983.

(7) Heimel, G.; Daghofer, M.; Gierschner, J.; List, E.; Grimsdale, A.; Müllen, K.; Beljonne, D.; Brédas, J.; Zojer, E. *J. Chem. Phys.* **2005**, *122*, 054501/1-054501/11.

(8) Pichler, K.; Halliday, D.; Bradley, D.; Burn, P.; Friend, R.; Holmes, A. *J. Phys.: Condens. Matter* **1993**, *5*, 7155.

(9) Cornil, J.; Beljonne, D.; Heller, C.; Campbell, I.; Laurich, B.; Smith, D.; Bradley, D.; Müllen, K.; Brédas, J. *Chem. Phys. Lett.* **1997**, *278*, 139.

(10) Gierschner, J.; Mack, H.; Lüer, L.; Oelkrug, D. *J. Chem. Phys.* **2002**, *116*, 8596.

(11) Hennebicq, E.; Pourtois, G.; Scholes, G. D.; Herz, L. M.; Russell, D. M.; Silva, C.; Setayesh, S.; Grimsdale, A. C.; Müllen, K.; Brédas, J. L.; Beljonne, D. *J. Am. Chem. Soc.* **2005**, *127*, 4744.

(12) Franco, I.; Tretiak, S. *J. Am. Chem. Soc.* **2004**, *126* (38), 12130.

(13) Grimme, J.; Scherf, U. *Macromol. Chem. Phys.* **1996**, *197* (7), 2297.

(14) DiCesare, N.; Belletête, M.; Garcia, E.; Leclerc, M.; Durocher, G. *J. Phys. Chem. A* **1999**, *103*, 3864.

(15) Rauscher, U.; Bassler, H.; Bradley, D. D. C.; Hennecke, M. *Phys. Rev. B* **1990**, *42*, 9830.

(16) Karabunarliev, S.; Baumgarten, M.; Müllen, K. *J. Chem. Phys. A* **2000**, *104* (35), 8236.

(17) Lax, M. *J. Chem. Phys.* **1952**, *20*, 1752.

(18) Hizhnyakov, V. *J. Phys. C: Solid State Phys.* **1987**, *20*, 6073.

(19) Keil, T. *Phys. Rev.* **1965**, 140 (2A), 601.

(20) Myers, A.; Trulson, M.; Mathies, R. *J. Chem. Phys.* **1985**, 83, 5000.

(21) Ziener, U.; Godt, A. *J. Org. Chem.* **1997**, *62* (18), 6137−6143.

(22) Kloppenburg, L.; Song, D.; Bunz, U. H. F. *J. Am. Chem. Soc.* **1998**, *120* (31), 7973−7974.

(23) Kloppenburg, L.; Jones, D.; Bunz, U. H. F. *Macromolecules* **1999**, *32* (13), 4194−4203.

(24) Halkyard, C. E.; Rampey, M. E.; Kloppenburg, L.; Studer-Martinez, S. L.; Bunz, Uwe H. F. *Macromolecules* **1998**, *31* (25), 8655−8659.

(25) Velapoldi, R.; Mielenz, K. *Standard Reference Materials: A Fluorescence Standard Reference Material: Quinine Sulfate Dihydrate*; U.S. Government Printing Office: Washington D.C., 1980.

(26) Jones, L., II; Schumm, J. S.; Tour, J. M. *J. Org. Chem.* **1997**, *62* (5), 1388−1410.

(27) Beeby, A.; Findlay, K.; Low, P. J.; Marder, T. B. *J. Am. Chem. Soc.* **2002**, *124* (28), 8280−8284.

(28) Somoza, M. I.; Andreatta, D.; Murphy, C. J.; Coleman, R. S.; Berg, M. A. *Nucleic Acids Res.* **2004**, *32*, 2494.

(29) Rossi, G.; Chance, R. R.; Silbey, R. *J. Chem. Phys.* **1989**, *90* (12), 7594−601.

(30) Frisch, M. J.; Trucks, G. W.; Schlegel, H. B.; Scuseria, G. E.; Robb, M. A.; Cheeseman, J. R.; Montgomery, J. A., Jr.; Vreven, T.; Kudin, K. N.; Burant, J. C.; Millam, J. M.; Iyengar, S. S.; Tomasi, J.; Barone, V.; Mennucci, B.; Cossi, M.; Scalmani, G.; Rega, N.; Petersson, G. A.; Nakatsuji, H.; Hada, M.; Ehara, M.; Toyota, K.; Fukuda, R.; Hasegawa, J.; Ishida, M.; Nakajima, T.; Honda, Y.; Kitao, O.; Nakai, H.; Klene, M.; Li, X.; Knox, J. E.; Hratchian, H. P.; Cross, J. B.; Bakken, V.; Adamo, C.; Jaramillo, J.; Gomperts, R.; Stratmann, R. E.; Yazyev, O.; Austin, A. J.; Cammi, R.; Pomelli, C.; Ochterski, J. W.; Ayala, P. Y.; Morokuma, K.; Voth, G. A.; Salvador, P.; Dannenberg, J. J.; Zakrzewski, V. G.; Dapprich, S.; Daniels, A. D.; Strain, M. C.; Farkas, O.; Malick, D. K.; Rabuck, A. D.; Raghavachari, K.; Foresman, J. B.; Ortiz, J. V.; Cui, Q.; Baboul, A. G.; Clifford, S.; Cioslowski, J.; Stefanov, B. B.; Liu, G.; Liashenko, A.; Piskorz, P.; Komaromi, I.; Martin, R. L.; Fox, D. J.; Keith, T.; Al-Laham, M. A.; Peng, C. Y.; Nanayakkara, A.; Challacombe, M.; Gill, P. M. W.; Johnson, B.; Chen, W.; Wong, M. W.; Gonzalez, C.; Pople, J. A. *Gaussian 03*, revision C.02; Gaussian, Inc.: Wallingford, CT, 2004.

(31) Samori, P.; Francke, V.; Enkelmann, V.; Müllen, K.; Rabe, J. P. *Chem. Mater.* **2003**, *15*, 1032−1039.

(32) Abramenkov, A. V.; Almenningen, A.; Cyvin, B. N.; Cyvin, S. J.; Jonvik, T.; Khaikin, S.; Romming, C.; Vilkov, L. V. *Acta Chem. Scand. Ser. A* **1988**, *42*, 674−684.

(33) Claudio, G. C.; Bittner, E. R. *Chem. Phys.* **2002**, *276*, 81−91.

(34) Dewar, M. J. S.; Zoebisch, E. G.; Healy, E. F.; Stewart, J. J. P. *J. Am. Chem. Soc.* **1985**, *107* (13), 3902−9.

(35) Tomlinson, A.; Yaron, D. *J. Comput. Chem.* **2003**, *24*, 1782−1788.

(36) Salem, L. *The Molecular Orbital Theory of Conjugated Systems*; W. A. Benjamin, Inc.: New York, 1966.

(37) Karelson, M.; Zerner, M. C. *Chem. Phys. Lett.* **1994**, *224* (1−2), 213−218.

(38) Hutchison, G. R.; Ratner, M. A.; Marks, T. J. *Polym. Mater.Sci. Eng.* **2001**, *85*, 609−610.

(39) Hill, I. G.; Kahn, A.; Cornil, J.; Dos Santos, D. A.; Brédas, J. L. *Chem. Phys. Lett.* **2000**, *317*, 444−450.

(40) Karabunarliev, S.; Baumgarten, M.; Bittner, E. R.; Müllen, K. *J. Chem. Phys.* **2000**, *113*, 11372.

(41) Moore, E. E.; Yaron, D. *J. Chem. Phys.* **1998**, *109* (14), 6147−6156.

(42) Brédas, J. L.; Cornil, J.; Beljonne, D.; Dos Santos, D. A.; Shuai, Z. *Acc. Chem. Res.* **1999**, *32*, 267.